Pelgrin, Vincent; Wang, Yuchen; Peltier, Jonathan; Alonso-Ramos, Carlos; Vivien, Laurent; Sun, Zhipei; Cassan, Eric

Boosting the SiN nonlinear photonic platform with transition metal dichalcogenide monolayers

Published in:
Optics Letters

DOI:
10.1364/OL.440462

Published: 15/02/2022

Document Version
Publisher's PDF, also known as Version of record

Please cite the original version:
Pelgrin, V., Wang, Y., Peltier, J., Alonso-Ramos, C., Vivien, L., Sun, Z., & Cassan, E. (2022). Boosting the SiN nonlinear photonic platform with transition metal dichalcogenide monolayers. *Optics Letters*, *47*(4), 734-737. https://doi.org/10.1364/OL.440462

Optics Letters

Boosting the SiN nonlinear photonic platform with transition metal dichalcogenide monolayers

VINCENT PELGRIN,[1,2,4] YUCHEN WANG,[2] JONATHAN PELTIER,[1] CARLOS ALONSO-RAMOS,[1] LAURENT VIVIEN,[1] ZHIPEI SUN,[2,3] AND ERIC CASSAN[1,5]

[1] Université Paris-Saclay, CNRS, Centre de Nanosciences et de Nanotechnologies, 91120, Palaiseau, France
[2] Department of Electronics and Nanoengineering, Aalto University, P.O. Box 13500, FI-00076 Aalto, Finland
[3] QTF Centre of Excellence, Department of Applied Physics, Aalto University, FI-00076 Aalto, Finland
[4] e-mail: vincent.pelgrin@universite-paris-saclay.fr
[5] e-mail: eric.cassan@universite-paris-saclay.fr

Received 18 August 2021; revised 25 November 2021; accepted 10 December 2021; posted 13 December 2021; published 2 February 2022

In the past few years, we have witnessed increased interest in the use of 2D materials to produce hybrid photonic nonlinear waveguides. Although graphene has attracted most of the attention, other families of 2D materials such as transition metal dichalcogenides have also shown promising nonlinear performance. In this work, we propose a strategy for designing silicon nitride waveguiding structures with embedded MoS_2 for nonlinear applications. The transverse geometry of the hybrid waveguide is optimized for high third-order nonlinear effects using optogeometrical engineering and multiple layers of MoS_2. Stacking multiple monolayers results in an improvement of two orders of magnitude compared to standard silicon nitride waveguides. The hybrid waveguide performance is then investigated in terms of four-wave mixing enhancement in micro-ring resonator configurations. A signal/idler conversion efficiency of −6.3 dB is reached for a wavelength of around 1.55 µm with a 5 mW pumping level.

https://doi.org/10.1364/OL.440462

Silicon photonics is a powerful platform in many respects, especially due to its possible CMOS compatibility. However, integrated silicon nonlinear optical applications at telecom wavelengths encounter a few difficulties. Although silicon is a very nonlinear material (Kerr index $n_2 \simeq 5 \times 10^{-18} \mathrm{m^2W^{-1}}$ [1]), its band structure induces two-photon absorption (TPA), thus strongly counterbalancing the optical Kerr nonlinearity of the material. Moreover, there is a limited choice of directly compatible materials for photonics. A classical alternative to silicon is silicon nitride (SiN). The absence of TPA in the near IR and the low propagation loss of SiN waveguides (below 1 dB/cm in the near-infrared) makes them of interest. Impressive demonstrations of supercontinuum generation [2,3] or frequency comb generation [4,5] have been reported on the SiN/SiO_2 platform. Yet, due to its relatively weak Kerr coefficient ($n_2 \simeq 2.4 \times 10^{-19} \mathrm{m^2W^{-1}}$; effective nonlinear coefficient $\gamma \approx 1\ \mathrm{W^{-1}\ m^{-1}}$ [6] versus a few hundred $\mathrm{W^{-1}\ m^{-1}}$ for Si/SiO_2 waveguides [7]), SiN necessitates the use of high-power pumps in order to meet the high power thresholds required to induce appreciable nonlinear effects (from several hundreds of mW up to a few W in continuous-wave power for the generation of broadband frequency combs [4,8]). One possible route to unlocking its potential is to turn to the emerging field of two-dimensional (2D) layered materials [e.g., graphene, black phosphorus, or transition metal dichalcogenides (TMDs)]. Recently, promising results for nonlinear frequency conversion using 2D materials have been demonstrated both in free space [for second-harmonic generation (SHG) and third-harmonic generation (THG) [9,10]] and in integrated photonics [with self-phase modulation (SPM) and four-wave mixing (FWM) [11,12]]. The idea is thus to exploit this family of materials to solve the limitations of standard SiN waveguides by relying on recent breakthroughs made in 2D material growth and transfer methods [13–15]. In this context, this Letter aims to optimize the integration strategies of 2D materials to boost the nonlinear properties of SiN waveguides at telecom wavelengths near to 1.5 µm while maintaining them TPA-free. Emphasis is placed on the waveguide mode group velocity dispersion profiles (critical for phase-matching conditions) and transverse field distributions. In a second step, we report on the optimization of the nonlinear properties of the hybrid waveguides, as well as on the calculation of the overlap between the transverse mode and the 2D material layers. Once the nonlinear waveguides are properly designed, the performance of a frequency conversion scheme is evaluated by considering a ring resonator configuration as a reference configuration to estimate the nonlinear photonic platform performance [16].

The properties of SiN waveguides in terms of both their linear (e.g., dispersion: effective index, group index) and nonlinear (nonlinear coefficient γ) properties are well known. Introducing new materials, even ultra-thin 2D materials, may affect the linear dispersion properties of the waveguides. It is important to know if this is the case and to be able to quantify it. Moreover, a detailed study of the waveguide dispersion is critical for designing the optimized structures because of the phase-matching requirements in nonlinear optical processes such as FWM [17]. In this study, MoS_2 was the preferred material as it presents appreciable performance in terms of nonlinear response and a large bandgap compared to other 2D materials, thus limiting two-photon absorption in the optical wavelength range of interest [10]. However, we note that other 2D materials could, in principle, also be considered for performance optimization using a similar strategy to the one proposed here. A commercial finite-difference eigenmode (FDE) mode solver was used and applied to a TMD-SiN hybrid waveguide in various configurations [see Fig. 1(a)]. The effect of one or several monolayers of MoS_2 was taken into account by considering the monolayer crystal to be a true 2D material modeled based on its surface conductivity σ_s for the calculation of waveguide modes [18]. The relative permittivity ϵ_r of the 2D material was expressed as a sum of N Lorentzian functions:

$$\epsilon_r = \frac{\epsilon(\omega)}{\epsilon_0} = 1 + \sum_{k=1}^{N} \frac{f_k}{\omega_k^2 - \omega^2 - i\omega\gamma_k} \quad (1)$$

The coefficients f_k, ω_k, and γ_k are specific to the material and were extracted by fitting experimental data for the most common TMDs (MoS_2, WS_2, $MoSe_2$, WSe_2) [19]. γ_k stands for the oscillator strength, ω_k is the resonance frequency, and γ_k the spectral width of the k $^{\text{th}}$ oscillator. The complex surface conductivity was then extracted from the dielectric function using the following expression:

$$\epsilon(\omega) = \epsilon_0 \left(1 + \frac{i\sigma_b}{\epsilon_0\omega}\right) = \epsilon_0 \left(1 + \frac{i\sigma_s}{\epsilon_0\omega h_{eff}}\right). \quad (2)$$

Related results are shown in Fig. 1(b) [18]. We based the study on SiN/SiO_2 waveguides operating at a wavelength range of approximately 1.0 and 2.0 μm while considering each material's dispersion with the Sellmeier equation [20,21]. Transverse electric (TE) polarization was considered for maximum interaction between the 2D material and the mode. Indeed, the base structure (displayed in Fig. 1) presents a higher overlap between the TE mode and the 2D material (0.026%) than for the TM mode (0.013%). The calculation was thus performed for various waveguide cross sections. The reference structure (without MoS_2) was given for comparison with the hybrid one (with MoS_2), which differed from the reference through the introduction of one or several MoS_2 monolayers (and later by additional oxide cladding).

The results obtained starting from a planarized SiN/SiO_2 buried strip with a height $h = 600$ nm and a width $w = 1000$ nm are displayed in Fig. 1. The introduction of the 2D material layer has little effect on both the transverse mode distribution (single-mode TE) and the waveguide dispersion properties [see Fig. 1(c)]. Therefore, no specific extra scheme is needed for light coupling between the two waveguide families because mode mismatch is not significant, thereby simplifying the design steps. This also makes the comparison between the reference uncladded SiN waveguides and the hybrid TMD-SiN ones more relevant. Both kinds of waveguides mainly differ only in propagation losses and nonlinearity strength. The literature reports several approaches for the integration of 2D materials [11,22,23]. 2D materials are usually transferred onto the chip using wet transfer methods [22]. However, once this has been accomplished, other operations can be undertaken. The deposition of an oxide layer such as Al_2O_3 or HfO_2 on top of the 2D material can be beneficial as it can act as a protective layer.

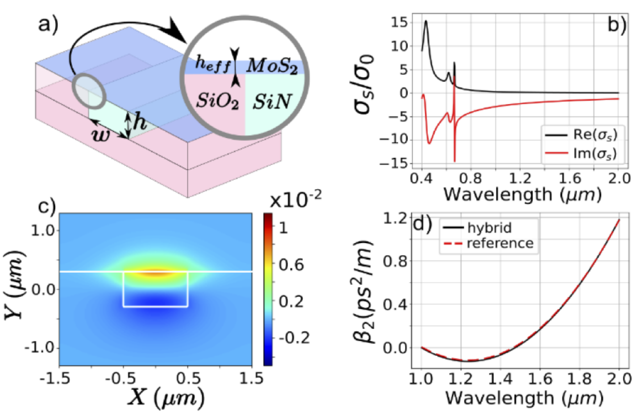

Fig. 1. (a) Studied structure with a 1000-nm-wide and 600-nm-high waveguide. (b) Calculated MoS_2 surface conductivity. (c) Comparison of the TE mode distributions of a reference structure (without MoS_2) and a structure covered with a monolayer of MoS_2 at $\lambda = 1.5$ μm. The represented field distribution is $E_{2D} - E_{ref}$ (the difference between the waveguide fields of the two structures). (d) Comparison of the related dispersion profiles.

In addition to this protective action, we propose to exploit this top cladding layer for another purpose. Because oxides such as Al_2O_3 or HfO_2, which can be grown easily using atomic layer deposition (ALD) [24], present linear refractive indices of 1.7 and 2.07, respectively, the added top cladding layer can improve the passive properties of the waveguide in terms of dispersion and directly contribute to increasing the nonlinear overlap between the 2D material layer and the transverse mode [see Fig. S1 in Supplement 1 and Eq. (3)]. Moreover, this approach does not introduce additional losses since those materials are transparent in the wavelength range of interest. A comparison of the results for hybrid MoS_2-SiN waveguides cladded or not with a 200 nm thick HfO_2 layer is displayed in Fig. S1 in Supplement 1 for the same base waveguide cross section ($w = 1000$ nm and $h = 600$ nm) as in Fig. 1. A shift in the dispersion profile appears, pushing the anomalous mode dispersion into the C band, and the spatial overlap factor of the guided quasi-TE mode changes from 0.03% to 0.08% with the addition of the HfO_2 cladding. The high-index top layer pulls the mode in the vertical direction. To quantify how this affects the nonlinearities, further studies were performed.

Estimation of the third-order nonlinear waveguide performance was achieved as follows [1]. With $e(r, \omega)$ being the TE profile and $\bar{e}(r, \omega)$ its complex conjugate, the effective nonlinear susceptibility of the structure is the result of the integral over the different components when considering the effective susceptibility tensor $\chi^{(3)}(r)$ of each considered material. Only SiN and the 2D layers were considered nonlinear; the other material (air, SiO_2) nonlinearities were neglected due to their relatively small nonlinear responses and the low mode confinement factor in those materials. Discrepancies in the $\chi^{(3)}$ of MoS_2 can be found in the literature. This is due to different fabrication methods and environmental deposition or growth conditions (either flake exfoliation or CVD (chemical vapor deposition) growth [9,10]). Thus, the n_2 value reported from integrated optics experiments performed at a wavelength of 1.55 μm for CVD-grown 2D materials was considered the most relevant reference ($n_2 = 1.1\times10^{-16}$ m^2 W^{-1} [11]). The needed in-plane susceptibility tensor component was then accounted for by considering the effective thickness of the monolayer h_{eff} [as depicted in Fig. 1(a)] while treating the 2D material as a thin 3D material and effectively accounting for the cross-section area occupied by MoS_2. The effective nonlinear susceptibility of the hybrid waveguides was thus estimated as [1]

$$\Gamma = \frac{A_0 \int_{A_{NL}} \bar{e}(r;\omega)\chi^{(3)}(r)e(r;\omega)\bar{e}(r;\omega)e(r;\omega)dA}{\left(\int_{A_\infty} n^2(r)|e(r;\omega)|^2 dA\right)^2}. \quad \textbf{(3)}$$

Here, A_0 is the waveguide core area, and A_{NL} is the cross section due to all of the materials participating in the waveguide effective nonlinearity. The susceptibility is related to the standard n_2 and the TPA coefficient (β_{TPA}) through the following relationship:

$$\frac{\omega}{c}n_2 + \frac{i}{2}\beta_{TPA} = \frac{3\omega}{4\epsilon_0 c^2 n^2}\chi^{(3)}. \quad \textbf{(4)}$$

TPA was subsequently ignored since it is absent from SiO_2 and SiN. Concerning the MoS_2 monolayers, the absence of TPA at $\lambda \approx 1.55\,\mu m$ was recently confirmed by theoretical studies [25]. The waveguide effective nonlinear susceptibility was then used to derive the effective nonlinear Kerr γ (approximately 1 $W^{-1}m^{-1}$ for a standard SiN waveguide) coefficient $\gamma = (3\omega\Gamma)/(4\varepsilon_0 A_0 v_g^2)$, where ε_0 is the permittivity in a vacuum and v_g is the group velocity of the propagating mode. This methodology was used to compare different approaches for optimizing nonlinear waveguides with embedded MoS_2 layers.

The main aim of the waveguide design was to consider the integration of a variable number of MoS_2 monolayers. To guarantee a realistic technological approach, the same planarized SiN waveguides as used in previous studies were considered. To ensure the monolayer character of the MoS_2, and thus the large bandgap of the material and an absence of TPA [25,26], we introduced TMD monolayers separated by Al_2O_3 spacers of a few nm: 5 nm was considered as a compromise between the safe isolation of single MoS_2 monosheets and a reasonably thin spacer to minimize the thickness of the whole material stack. The proposed approach is compatible with the growth of all materials (TMD, Al_2O_3 spacers, HfO_2) through ALD [24]. The aim of the study was to present a general structure that can later be improved based on particular requirements (e.g., Al_2O_3 and HfO_2 can be replaced by other materials). As an intermediate illustrative step, Fig. 2 shows the results obtained for a MoS_2 bilayer stack on top of the reference SiN planarized waveguide already considered in Figs. 1 and S1 in Supplement 1. The bilayer stack was covered by a 200 nm HfO_2 cap to steer the optical mode upward and increase the overlap with the MoS_2 2D monolayers.

Figure 2(b) shows the nonlinear coefficient γ calculated with Eq. (S1) (see Supplement 1) for varying cross-section dimensions; a fivefold increase in γ is observed upon varying the cross-section dimensions. The same trend can be observed in Fig. 2(c) for the overlap between the MoS_2 and the TE mode. Comparison of Fig. 2(c) and Fig. 2(d) suggests that the γ increase is directly related to the increase in the mode/TMD layer overlap. Obviously, the number of layers can thus be further increased, which is supported by very convincing feasibility arguments concerning the possibility of stacking a series of 2D material sheets [16]. The related results are displayed in Fig. 3. Again, a 200 nm layer of HfO_2 is placed on top of the SiN/MoS_2 to attract the mode upward. This introduces an impressive boost to the effective nonlinear coefficient γ, with an increase of about two orders of magnitude for the maximum value when compared with a standard SiN planarized buried strip. Saturation of the improvement above a certain number of layers (e.g., 40) is also observed. At some point, the optical mode spreads too much, causing a decrease in the field density around the 2D material

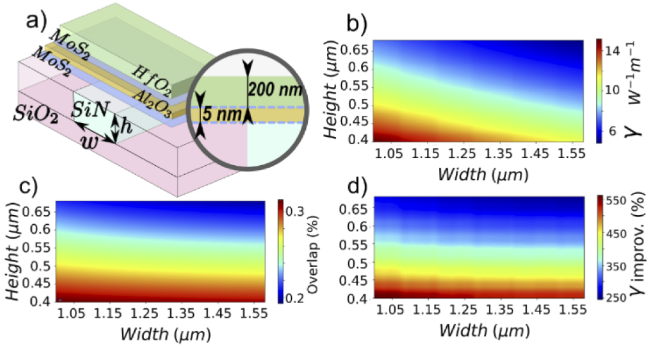

Fig. 2. (a) SiN planarized buried strip covered with two MoS_2 monolayers. (b) Plot of the nonlinear effective coefficient γ versus the dimensions of the waveguide (height and width). (c) Overlap between the 2D materials and the TE mode corresponding to the confinement factor of the mode inside MoS_2. (d) Improvement factor.

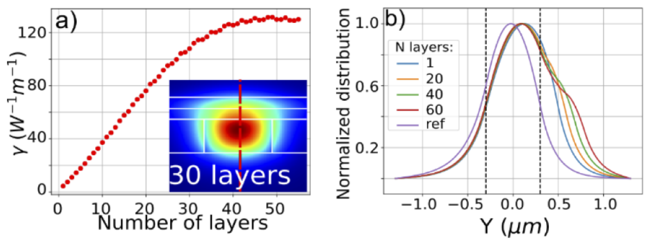

Fig. 3. (a) Effective nonlinear coefficient (γ) versus the number of layers (each additional layer, including an Al_2O_3 spacer, brings another 5 nm of thickness added on top). (b) Slice of the TE mode taken along the dashed vertical line (inset). The dashed black lines represent the core boundaries: reference corresponds to standard planarized buried SiN waveguide.

layers. However, this limitation sets a very comfortable limit on the optimization of the hybrid TMD-SiN waveguides, with nonlinear coefficients reaching values of more than 100 W^{-1} m^{-1} . This approach yields to performance comparable to Si waveguides [7] while further TPA-free telecom wavelengths.

Subsequently, we turned our interest to an emblematic application with the enhanced waveguide nonlinearity. We chose wavelength conversion by degenerate FWM in a ring resonator structure based on the previously optimized hybrid waveguides. This device is an all-pass resonator device, and is presented in Fig. 4(b). For this study, we relied on a formalism developed and described in several previous papers and presented in Supplement 1. The conversion efficiency was calculated for two devices with identical cross-sections but different settings: one a straight waveguide and the other a regular micro-ring with a 100 μm radius, with the considered unfolded propagation lengths set to the same value to enable a comparison of the designs. Those results are presented in Fig. 4 for degenerate FWM processes around a wavelength of 1.55 μm. The pump power considered in this study was 5 mW, a reasonably low power level for a continuous-wave pumped optical source. The calculations were performed for frequencies at neighboring resonances [see Fig. 4(a)]. The comparison was made using different parameters as variables. The different types of waveguide designs translate into different effective nonlinear γ factors. The $\gamma \approx 1\,W^{-1}$ m^{-1} case corresponds to a standard reference

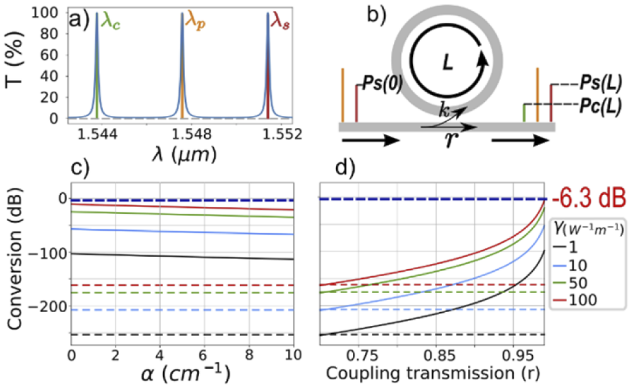

Fig. 4. (a) Transfer function of a 100-μm-radius ring resonator around 1.55 μm. (b) Ring resonator coupling area. k and r are the cross and pass coefficients, respectively. $P_S(0)$, $P_S(L)$, $P_C(L)$ are the input, the output, and the output converted (idler) powers. (c) and (d) Conversion efficiency η in dB for straight waveguides (dashed lines) and rings (full lines). In (c), η is plotted versus the propagation loss ($r = 0.99$); (d) plots η versus r (for $\alpha = 0.7\ \mathrm{cm}^{-1}$).

SiN buried-strip planarized waveguide without additional active material. The three other values are for low, medium, and high values of the showcased structure of Fig. 2. It is apparent that a strong transmission coefficient is required from the coupling area of the waveguide to make the effect of the ring interesting. This is expected when considering that a high-quality factor can be linked to a high photon lifetime in the cavity. Moreover, for a ring with high coupling transmission, the conversion efficiency remains higher for the ring than for the straight waveguide, even for very high loss levels. However, as the propagation losses increase, the overall quality factor is reduced, reducing the conversion efficiency faster than in a straight waveguide. In any case, using an appropriate design (high coupling transmission) yields a conversion efficiency as high as −6.3 dB (see Fig. 4), which compares well to those obtained in similar studies conducted on the silicon on insulator (SOI) platform [27].

To conclude, we propose a novel approach for boosting the nonlinear photonic SiN/SiO_2 platform through the proper integration of MoS_2 monolayers in SiN planarized waveguides. The strategy relies on dispersion engineering and optimizing the waveguide structure to maximize the interaction between the TE mode and MoS_2. Using multiple monolayers of MoS_2 separated by oxide spacers, and by pulling the mode vertically by including a high-index dielectric layer of cladding on the top, we have designed TPA-free hybrid photonic waveguides with effective nonlinear coefficients of up to $\gamma \sim 120\ \mathrm{W}^{-1}\ \mathrm{m}^{-1}$. Micro-ring resonators relying on these optimized nonlinear waveguides show the potential for wavelength conversion efficiencies reaching −6.3 dB for pump power levels as low as 5 mW at a wavelength of 1.55 μm. The proposed approach will provide useful guidelines for further development of integrated nonlinear optics and its applications, such as frequency combs and supercontinuum generation relying on the integration of 2D materials in the SiN platform.

Funding. Université Paris-Saclay; Aalto-Yliopisto.

Acknowledgments. This work was supported by Paris Saclay University within the C2N in France and Aalto University in Finland.

Disclosures. The authors declare no conflicts of interest.

Data availability. Data underlying the results presented in this paper are not publicly available at this time but may be obtained from the authors upon reasonable request.

Supplemental document. See Supplement 1 for supporting content.

REFERENCES

1. R. M. Osgood, N. C. Panoiu, J. I. Dadap, X. Liu, X. Chen, I. W. Hsieh, E. Dulkeith, W. M. J. Green, and Y. A. Vlasov, Adv. Opt. Photonics **1**, 162 (2009).
2. A. R. Johnson, A. S. Mayer, A. Klenner, K. Luke, E. S. Lamb, M. R. E. Lamont, Y. Okawachi, F. W. Wise, M. Lipson, U. Keller, and A. L. Gaeta, Opt. Lett. **40**, 5117 (2015).
3. R. Halir, Y. Okawachi, J. S. Levy, M. A. Foster, M. Lipson, and A. L. Gaeta, Opt. Lett. **37**, 1685 (2012).
4. M. H. P. Pfeiffer, C. Herkommer, J. Liu, H. Guo, M. Karpov, E. Lucas, M. Zervas, and T. J. Kippenberg, Optica **4**, 684 (2017).
5. V. Brasch, M. Geiselmann, T. Herr, G. Lihachev, M. H. P. Pfeiffer, M. L. Gorodetsky, and T. J. Kippenberg, Science **351**, 357 (2016).
6. D. J. Moss, R. Morandotti, A. L. Gaeta, and M. Lipson, Nat. Photonics **7**, 597 (2013).
7. R. Salem, M. A. Foster, A. C. Turner, D. F. Geraghty, M. Lipson, and A. L. Gaeta, Nat. Photonics **2**, 35 (2008).
8. T. Herr, K. Hartinger, J. Riemensberger, C. Y. Wang, E. Gavartin, R. Holzwarth, M. L. Gorodetsky, and T. J. Kippenberg, Nat. Photonics **6**, 480 (2012).
9. A. Autere, H. Jussila, A. Marini, J. R. M. Saavedra, Y. Dai, A. Säynätjoki, L. Karvonen, H. Yang, B. Amirsolaimani, R. A. Norwood, N. Peyghambarian, H. Lipsanen, K. Kieu, F. J. G. De Abajo, and Z. Sun, Phys. Rev. B **98**, 115426 (2018).
10. A. Autere, H. Jussila, Y. Dai, Y. Wang, H. Lipsanen, and Z. Sun, Adv. Mater. **30**, 1705963 (2018).
11. L. Liu, K. Xu, X. Wan, J. Xu, C. Y. Wong, and H. K. Tsang, Photonics Res. **3**, 206 (2015).
12. Y. Zhang, L. Tao, D. Yi, J. Bin Xu, and H. K. Tsang, J. Opt. **22**, 025503 (2020).
13. S. Najmaei, Z. Liu, W. Zhou, X. Zou, G. Shi, S. Lei, B. I. Yakobson, J. C. Idrobo, P. M. Ajayan, and J. Lou, Nat. Mater. **12**, 754 (2013).
14. S. Li, Y. C. Lin, W. Zhao, J. Wu, Z. Wang, Z. Hu, Y. Shen, D. M. Tang, J. Wang, Q. Zhang, H. Zhu, L. Chu, W. Zhao, C. Liu, Z. Sun, T. Taniguchi, M. Osada, W. Chen, Q. H. Xu, A. T. S. Wee, K. Suenaga, F. Ding, and G. Eda, Nat. Mater. **17**, 535 (2018).
15. M. Liao, Z. Wei, L. Du, Q. Wang, J. Tang, H. Yu, F. Wu, J. Zhao, X. Xu, B. Han, K. Liu, P. Gao, T. Polcar, Z. Sun, D. Shi, R. Yang, and G. Zhang, Nat. Commun. **11**, 2153 (2020).
16. J. Wu, Y. Yang, Y. Zhang, Y. Qu, L. Jia, X. Xu, S. T. Chu, B. E. Little, R. Morandotti, B. Jia, and D. J. Moss, in *14th Pacific Rim Conference on Lasers and Electro-Optics (CLEO PR 2020)*, (2020), paper C11E_4.
17. G. P. Agrawal, in *Nonlinear Science at the Dawn of the 21st Century* (Springer, 2000) pp. 195–211 .
18. M. Weismann and N. C. Panoiu, Phys. Rev. B **94**, 035435 (2016).
19. Y. Li, A. Chernikov, X. Zhang, A. Rigosi, H. M. Hill, A. M. Van Der Zande, D. A. Chenet, E. M. Shih, J. Hone, and T. F. Heinz, Phys. Rev. B **90**, 205422 (2014).
20. K. Luke, Y. Okawashi, M. R. E. Lamont, A. L. Gaeta, and A. M. Lipson, Opt. Lett. **40**, 4823 (2015).
21. I. H. Malitson, J. Opt. Soc. Am. **55**, 1205 (1965).
22. I. Datta, S. H. Chae, G. R. Bhatt, M. A. Tadayon, B. Li, Y. Yu, C. Park, J. Park, L. Cao, D. N. Basov, J. Hone, and M. Lipson, Nat. Photonics **14**, 256 (2020).
23. B. Yao, S. W. Huang, Y. Liu, A. K. Vinod, C. Choi, M. Hoff, Y. Li, M. Yu, Z. Feng, D. L. Kwong, Y. Huang, Y. Rao, X. Duan, and C. W. Wong, Nature **558**, 410 (2018).
24. S. Franssila, John Wiley Sons (2010).
25. Y. Z. Lan and X. H. Bao, Phys. Rev. B **101**, 155422 (2020).
26. H. S. Lee, S. W. Min, Y. G. Chang, M. K. Park, T. Nam, H. Kim, J. H. Kim, S. Ryu, and S. Im, Nano Lett. **12**, 3695 (2012).
27. Z. Li, S. Gao, Q. Liu, and S. He, Opt. Commun. **284**, 2215 (2011).